# Catalysis Science & Technology

Accepted Manuscript






ROYAL SOCIETY OF CHEMISTRY

www.rsc.org/catalysis

Journal Name

RSCPublishing

ARTICLE

# Flower-like Au/Ni-Al Hydrotalcite with Hierarchical Pore Structure as a Multifunctional Catalyst for Catalytic Oxidation of Alcohol

Y. Y. Du, Q. Jin, J. T. Feng*, N. Zhang, Y. F. He, D. Q. Li*

Cite this: DOI: 10.1039/xoxxoooooox

Received ooth January 2012,
Accepted ooth January 2012

DOI: 10.1039/xoxxoooooox

www.rsc.org/

Flower-like hierarchical Au/NiAl-LDH catalysts were synthesized for selective oxidation of alcohols. Abundant hydrogen vacancies at the edge of flowers as the nucleation center made contributions for the uniform dispersion of AuNPs. The confinement effect of the hierarchical pores promoted 60% higher activity than the common Au/NiAl-LDH nanoparticle catalyst in the oxidation of benzyl alcohol by heightening the effective collisions between substrates and active sites. The evolution process of hierarchical pores in support was further proposed. Moreover, the reaction mechanism of the cooperation among Brønsted base sites, $Ni^{III}$ coordinatively unsaturated metal sites and isolated gold cations was concretely proved. In the oxidation of other typical alcoholic substrates, the flower-like catalyst kept higher activity than the common nanoparticle one except for linear alcohols, which could be attributed to the shape selectivity of straight macro-pores.

## Introduction

Liquid phase oxidation of alcohols is of great importance and preferred for the environment-friendly synthesis of aldehydes without generation of greenhouse gas $CO_2$. In the mechanism of alcoholic oxidation, β-H fracture is generally accepted as the determined step. It has been widely considered that the addition of alkali can efficiently enhance the catalytic activity by accelerating this step. However, it is not an environment-friendly way due to the difficulties in separation. Solid base supports which possess abundant hydroxyls are therefore desirable in the base-free oxidation of alcohols in view of green and sustainable chemistry. Layered double hydroxide (LDH), known as a family of synthetic anionic clays, are a class of two-dimensional brucite $Mg(OH)_2$-like layered inorganic materials. In the general formula of $[M^{2+}_{1-x}M^{3+}_{x}(OH)_2]^{x+}(A^{n-})_{x/n}\cdot mH_2O$, $M^{2+}$ locates on the layers substituted by $M^{3+}$ partially with regular hydroxyl arrays, $A^{n-}$ acts as balancing anions in the interlayer space with water molecules. As a consequence of the tailored structure-design, LDHs and their calcined products mixed metal oxides (MMO) with tunable acidic and basic properties can provide extremely potential opportunities for designing and innovating novel catalytic supports in the base-free oxidation of alcohols.[1-4] Very recently, we reported the research on the novel heterogeneous catalyst which combined acid–base bifunctional material of MgAl-MMO with bimetallic AuPd nanoparticles for solvent-free oxidation of benzyl alcohol (BA) and exhibited dramatic performance.[3] However, in view of the high price and less reserve of noble metals, the alternation of one metal with non-noble one is more potential in the application of oxidized catalysts.

Gold nanoparticles (AuNPs) demonstrate high selectivity in heterogeneous selective liquid oxidations[5, 6] but lower activity compared with other noble metallic nanoparticles especially PdNPs[7-10]. Recently, there has been a growing interest in the design and synthesis of efficient Au-based catalysts synergized by reducible supports with transition metals such as Cr[2], Mn[11] and Ni[12-14]. Liu et al.[2] reported the application of CrMgAl-LDH supported Au catalyst and revealed the strong Au-Cr synergy which was related to a $Cr^{3+} \leftrightarrow Cr^{6+}$ redox cycle at the Au/CrMgAl-LDH interface, where $O_2$ activation took place accompanied with electron transfer from CrMgAl-LDH to Au. However, Au-based catalysts supported by LDHs with other reducible metals are rarely reported. Comparing with other reducible metals, the application of Ni-based support with hypotoxicity and efficiency is more significantly in accordance with the main tendency of green chemistry.

The property of easy aggregation for nanomaterials in liquid reactions is an undeniable fact. Preparing micro-level hierarchical materials is considered as an effective way to solve this problem. This kind of materials can inherit many properties from building units such as high surface area and a large amount of active sites and generate some new characteristics such as specific internal porosity, plentiful coordinatively unsaturated metal sites (CUS) and outstanding separation and recirculation ability. Yu et al.[15] fabricated hollow spherical

$CeO_2$ supported Au catalyst which showed high activity and a long lifetime in the catalytic reduction of *p*-nitrophenol because of the nanosized interconnected chambers of the hierarchical support resulting in the large specific surface area and narrow mesopore distribution. Zhang et al.[4] assembled MgAl-LDH nanosheets onto the magnetic $Fe_3O_4$ cores for the preparation of the Au/LDH/$Fe_3O_4$ catalyst. The outer honeycomb-like microstructure of the obtained core-shell $Fe_3O_4$@LDH nanospheres provided abundant accessible edges and junction sites of LDH crystals. Besides, perpendicularly interlaced MgAl-LDH nanocrystals facilitated the immobilization of AuNPs along with avoiding the possible aggregation. However, it is rarely reported the catalyst which simultaneously contains the superiorities of hierarchical materials and the advantages of rich hydroxy in LDHs, as well as the strong synergy between reducible metal species and Au in the oxidation of alcohols. Therefore, we designed and fabricated flower-like NiAl-LDH microparticles as the multifunctional support for Au catalyst. The catalytic performance of as-fabricated flower-like Au/NiAl-LDH catalyst was evaluated through various alcoholic oxidations with molecular $O_2$ and BA oxidation was chosen as the probe reaction to investigate the structure-performance relationships. By comparing with the common nanoparticle catalyst, the structural effect of flower-like catalysts in the catalytic performance was revealed. Furthermore, the synergistic effect between Ni and Au was also evaluated by identifying the oxidation states and the redox process. The rational reaction mechanism and route were further clarified.

## Results and discussion

### Characterization and catalytic activities of various catalysts

The SEM images of NiAl-LDH-P-36 and NiAl-LDH-F-36 are shown in Fig. 1(a) and (b). In NiAl-LDH-P-36, shapeless aggregations are observed. Correspondingly, the flower-like structure with outer trumpet-like pores is obviously demonstrated in NiAl-LDH-F-36. The well-defined layered structure characteristic of pure hydrotalcite was confirmed by

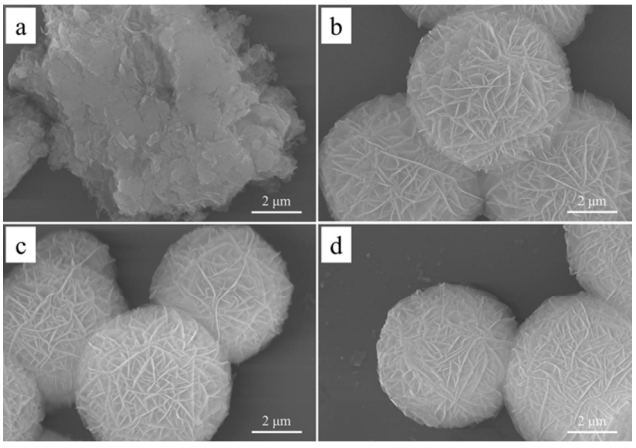


**Fig. 1** SEM images of NiAl-LDH-P-36 (a), NiAl-LDH-F-36 (b), NiAl-LDH-F-24 (c) and NiAl-LDH-F-12 (d).

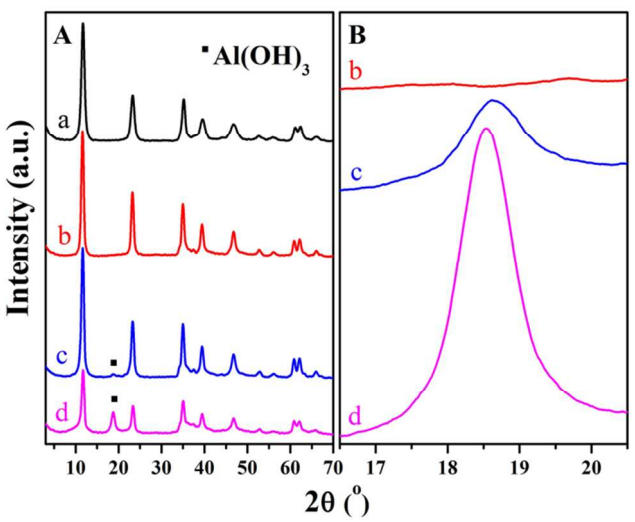


**Fig. 2** XRD patterns (A) of NiAl-LDH-P-36 (a), NiAl-LDH-F-36 (b), NiAl-LDH-F-24 (c) and NiAl-LDH-F-12 (d) precursors and partial enlarged views (B) from 16.5° to 20.5°.

XRD analysis in Fig. 2A(a) and (b) for NiAl-LDH-P-36 and NiAl-LDH-F-36, respectively.[17]

HRTEM images of AuNPs dispersed on NiAl-LDH-P-36 and NiAl-LDH-F-36 supports are shown in Fig. 3(a), (b), (d) and (e) in which low-magnification images are on the left and high-magnification ones are in the middle. From low-magnification images, the AuNPs distribute more evenly on the surface of the NiAl-LDH-F-36 (Fig. 3(d)) than on NiAl-LDH-P-36 (Fig. 3(a)). It is worth noticing that, in Au/NiAl-LDH-F-36 catalyst, AuNPs are more inclined to load near the edge of the "flowers petals" with the distance range of around 150 nm from the edges where locate abundant CUS as "dangling orbital" with high densities leading to larger cohesive energy than that on the top site for the preferential deposition of AuNPs.[18] The corresponding particle size distributions by measuring more than 200 particles from different regions are also shown in Fig. 3. The AuNPs size distributions and average sizes (Au/NiAl-LDH-P-36 2.44 nm and Au/NiAl-LDH-F-36 2.45 nm) are both similar in Au/NiAl-LDH-P-36 and Au/NiAl-LDH-F-36. Furthermore, there is no visible difference in the morphology of metal nanoparticles.

The catalytic performances of as-synthesized Au/NiAl-LDH-P-36 and Au/NiAl-LDH-F-36 catalysts were tested in the oxidation of BA. The catalytic data are listed in Table 1. Benzaldehyde (BD) was the predominant product (the selectivity≥99%) in all cases. The turnover frequency (TOF) and BD yield of the flower-like Au/NiAl-LDH-F-36 catalyst both perform nearly 60% higher than Au/NiAl-LDH-P-36. In order to investigate the factors for the increase of activity, ICP and MIP were carried out. From the composition analysis, Ni/Al molar ratios as well as the Au loading of Au/NiAl-LDH-P-36 and Au/NiAl-LDH-F-36 are very close to the feeding ratio (3.0:1.0 and 1.0 wt%). Therefore, it can be surmised that the enhancement of activity in Au/NiAl-LDH-F-36 is mainly due to the structural effect of supports. In NiAl-LDH-P-36, pores are formed mainly by the aggregation of NiAl-LDH nanoparticles,

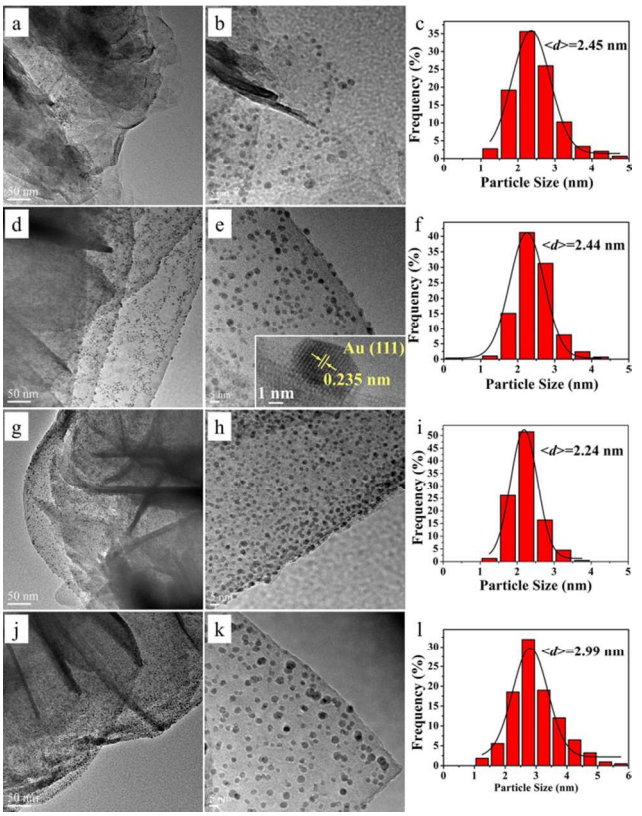


**Fig. 3** HRTEM images and AuNPs size distributions of Au/NiAl-LDH-P-36 (a-c), Au/NiAl-LDH-F-36 (d-f), Au/NiAl-LDH-F-24 (g-i) and Au/NiAl-LDH-F-12 (j-l). The low-magnification images (a, d, g and j) are on the left. The high-magnification images (b, e, h and k) are in the middle. The AuNPs size distributions (c, f, I and l) are on the right.

which is obviously different from that in NiAl-LDH-F-36 circled by "flower petals". In order to investigate the structural transformation in the growth process of flower, we thus synthesized flower-like catalysts with reduced hydrothermal duration of 24 h and 12 h for researching the structure-performance relationships.

**Structural effect of support on catalytic performance**

The AuNPs morphology of Au/NiAl-LDH-F-24 and Au/NiAl-LDH-F-12 are shown in Fig. 3(g), (h), (j) and (k). Similar with Au/NiAl-LDH-F-36 catalyst, AuNPs in Au/NiAl-LDH-F-24 and Au/NiAl-LDH-F-12 with ~1 wt% loadings also locate at the edge of "flower petals" with the average size of 2.99 nm and 2.24 nm, respectively. In the test of BA oxidation, interestingly, the trend of activities is proportional to the hydrothermal duration. Therefore, we speculate that the activity could be related to the structural evolution of the pores in supports.

In Fig. 1(c) and (d), trumpet-like microstructure of NiAl-LDH-F-24 and NiAl-LDH-F-12 can also be obviously observed. However, with the extension of hydrothermal duration, slight morphological distinguishes appear especially in the size of "flower petals" and the depth of pores. Significantly, an individual structure of solid "core-petal" can be recognized in NiAl-LDH-F-12, which is different from NiAl-LDH-F-24 and NiAl-LDH-F-36 with no obvious solid cores. Furthermore, the pores circled by "petals" become deeper followed by the extension of hydrothermal duration. For accurately investigating the evolution process and extent of "flower petals" and pores in hydrothermal procedure, XRD, ICP and MIP analysis were carried out.

**Table 1** Aerobic oxidation of benzyl alcohol over various Au/NiAl-LDH catalysts.[a]

| Catalyst | S ($m^2/g$)[b] | Ni/Al molar ratio[c] | [Au] (wt%)[c] | $d_{Au}$ (nm) | Yield (%)[d] | TOF ($h^{-1}$)[e] |
|---|---|---|---|---|---|---|
| Au/NiAl-LDH-P-36 | 42 | 2.99:1.0 | 1.00 | 2.45 | 34 | 267 |
| Au/NiAl-LDH-F-36 | 70 | 3.07:1.0 | 0.99 | 2.44 | 53 | 423 |
| Au/NiAl-LDH-F-24 | 64 | 3.31:1.0 | 0.98 | 2.24 | 36 | 286 |
| Au/NiAl-LDH-F-12 | 61 | 1.32:1.0 | 1.00 | 2.99 | 25 | 199 |
| NiAl-LDH-F-36 | 70 | 3.07:1.0 | - | - | 2 | - |
| Au/MgAl-LDH-P-36 | 12 | 3.00:1.0[i] | 0.99 | 2.46 | 13 | 103 |
| Au/NiAl-LDH-F-36[f] | 70 | 3.07:1.0 | 0.99 | 2.44 | 13 | 104 |
| Au/NiAl-LDH-P-36[g] | 42 | 2.99:1.0 | 0.94[h] | 4.58[h] | 30 | 235 |
| Au/NiAl-LDH-F-36[g] | 70 | 3.07:1.0 | 0.99[h] | 3.48[h] | 51 | 409 |

[a] Reaction conditions: benzyl alcohol (1 mmol), catalysts (0.05 g), toluene (10 mL), $O_2$ bubbling (20 mL $min^{-1}$), 100 °C, 0.5 h.

[b] Determined by MIP.

[c] Determined by ICP.

[d] Yields of BD were determined by GC-FID.

[e] Turnover frequency based on BD yield and gold loading for 0.5 h, and given in $mol_{BD}$ $mol_{total\ Au}^{-1}$ $h^{-1}$.

[f] Without pre-treated by calcining in air.

[g] Oxidation results for the 3rd run.

[h] Corresponding data after 3rd run.

[i] Mg/Al molar ratio.

In Fig. 2A(c) and (d), there are phase separation phenomenon in NiAl-LDH-F-24 and NiAl-LDH-F-12 at around 2θ 18.8° arising from a few $Al(OH)_3$ (PDF No. 74-1119). In the partial enlarged views (Fig. 2B), the peak intensity of $Al(OH)_3$ phase drops gradually with the extension of synthesized duration until disappears at 36 h. Additionally, the actual ratio of Ni/Al in NiAl-LDH-F-12 (1.32:1.0) is evidently lower than the theoretical value (3.0:1.0). However, it approaches 3.0:1.0 after 36 h.

Pore distributions were investigated by MIP and BET as shown in Fig. 4 and Fig. S1, respectively. In the support of NiAl-LDH-P-36, all the pores are in the range of meso-scale (below 50 nm). The NiAl-LDH-F-36 support also has abundant meso-pores and the pore distribution in meso-scale is almost identical with NiAl-LDH-P-36 as shown in Fig. S1(A). From the BET analysis, the structures of the meso-pores in NiAl-LDH-P-36 and NiAl-LDH-F-36 are similar as shown in Fig. S1(B), which means the adsorption processes in meso-pores for substrates have no obvious differences in these two catalysts.[19] Besides, the NiAl-LDH-F-36 support possesses a number of macro-pores in the range of 170 nm~1 μm, which can be regarded as abundant micro-spaces separated by "flower petals" and increase not only the accessibility of active sites but also the chance for effective collisions between substrates and active sites.[20, 21] Therefore, it can be conjectured that the confinement effect of hierarchical pores is the key factor for the enhancement of activity in Au/NiAl-LDH-F-36 for BA oxidation. Significantly, in Fig. 4(c) and (d), the maco-pores in NiAl-LDH-F-24 and NiAl-LDH-F-12 exhibit similar bimodal distributions with the same peak positions around 210 nm and 520 nm. However, in NiAl-LDH-F-36, the peak at 520 nm tends to shift to nearly 380 nm as shown in Fig. 4(b), which could be attributed to the growth of abundant new "petals" among the old ones from 24 h to 36 h leading to the separation of the original pores.

Based on above results, the growth process of as-synthesized flower-like NiAl-LDH is proposed as the scheme 1. At beginning, $Al^{3+}$ ions are rapidly precipitated because of the hydrolysis of urea, leading to the formation of spherical $Al(OH)_3$ cores as observed in SEM and XRD. Meanwhile, $Ni^{2+}$ is complexed by $F^-$. With the slow slight release of $Ni^{2+}$ ions and further formation of NiAl-LDH crystal in 12 h, a dramatic change in morphology occurres. Tiny NiAl-LDH "petals" grow out on the surface of $Al(OH)_3$ spheres by *in situ* growth along with the appearance of macro-pores as the initial morphology of flowers in Fig. 1(d). Subsequently, the release of massive $Ni^{2+}$ ions accompanies with the dissolution of $Al(OH)_3$ by alkaline condition, which results in not only the extension of NiAl-LDH platelets but also the shrink of $Al(OH)_3$ spheres as mentioned above in SEM analysis. At this time, the acquired $F^-$ ions from the dissociation of complexes adsorb on the {001} facets and perform as the capping agent, which suppresses the growth of LDH along *c*-axis leading to the extension of flower "petals". This speculation is similar with that in the literature.[22] The gradual increase of surface area accompanied with the extension of hydrothermal duration in flower-like NiAl-LDH support is the powerful testimony for the growth of LDH platelets and the deepening of pores. Significantly, much higher Ni/Al actual molar ratio of 3.31:1.0 determined by ICP analysis compared to theoretical value in NiAl-LDH-F-24 suggests that the dissolution rate of $Al(OH)_3$ exerts faster than the releasing rate of $Ni^{2+}$ ions. When the hydrothermal time reaches 36 h, almost all $Ni^{2+}$ and $Al^{3+}$ enter into the layers of NiAl-LDH, which has been confirmed by XRD and ICP. No characteristic diffraction peaks of $Al(OH)_3$ can be observed by XRD and the Ni/Al molar ratio approaches to the theoretical value. In the analysis of pore structure, the decrease of pore size along with the increase of surface area beyond 24 h is caused by the growth of new "petals" among old ones, which separates more microspaces and therefore leads to an increase in activity.

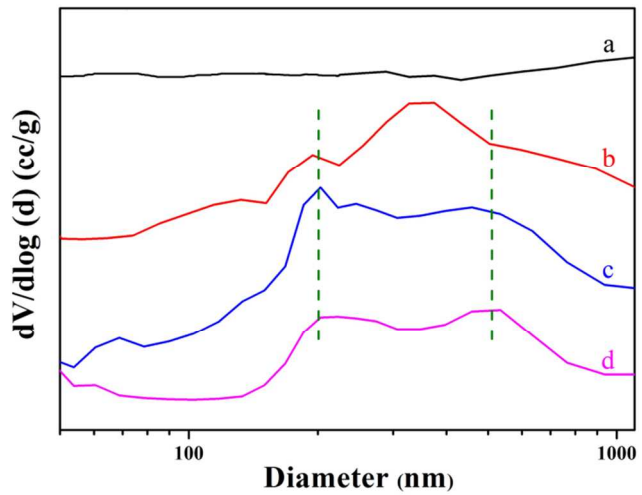


**Fig. 4** Pore size distributions of NiAl-LDH-P-36 (a), NiAl-LDH-F-36 (b), NiAl-LDH-F-24 (c) and NiAl-LDH-F-12 (d).

### Synergistic effect of Au and Ni

To investigate more information on the reaction mechanism, some contrastive catalysts were test by BA oxidation as shown in Table 1. Considering with the influence of support composition, MgAl-LDH supported Au catalyst was synthesized similarly with Au/NiAl-LDH-P-36 catalyst (Fig. S2

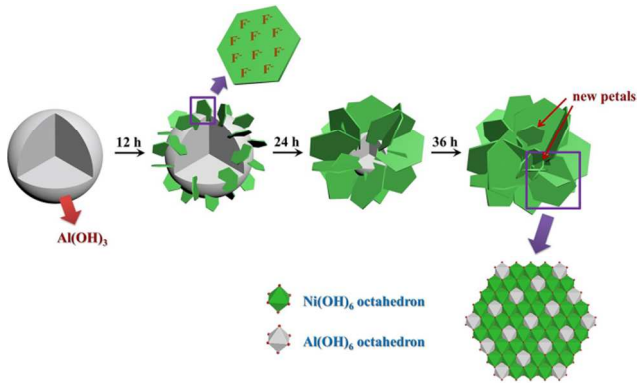


**Scheme 1** Schematic representation for the growth process of flower-like NiAl-LDH.

and S3). In comparison with Au/NiAl-LDH-P-36, 60% lower activity is performed in Au/MgAl-LDH-P-36, which confirms the support is of importance in respect to the origin of the catalyst activity. However, the pristine NiAl-LDH is almost inactive in our case. Hence, the benefit of utilizing the NiAl-LDH as a support can be attributed to the synergistic effect between Ni and Au. In general, pretreating process can also affect the performance of catalysts. In the test of non-pretreated Au/NiAl-LDH-F-36, 75% lower activity than the pretreated one implies the importance of oxidized states in this hybrid system for the enhancement of activity after calcination. Concentrating above, the synergy between Au and Ni was further researched by surveying the oxidized states and verifying the main reaction center in this hybrid system.

XPS were examined on the fresh, pretreated and recycled Au/NiAl-LDH-F-36 catalysts and NiAl-LDH-F-36 support as shown in Fig. 5A and B, respectively and the relative fractions of the species in Ni $2p_{3/2}$ and Au $4f_{7/2}$ are listed in Table S1. In all cases, the FWHM was constrained to be equal in each sample for all deconvoluted peaks from photoemission spectra of the same species using an 80%/20% Gaussian/Lorentzian sum and a Shirley background. The curves of Au 4f electron were fitted well to double groups of peaks, corresponding to $4f_{7/2}$ and $4f_{2/5}$, respectively, with the same peak area ratio (4:3) in per pair of corresponding peaks. By comparison, it is worth mentioning that a wide band is obviously obtained at 852.85 eV in the fresh pure LDH which is attributable to unsaturated $Ni^{2+}$-O lattice species[13], however, it disappears after loading AuNPs. Therefore, we speculate that Au atoms locate on the support surface through the Au-O-Ni model, which indicates that the hydrogen vacancies as a kind of CUS on the surface of NiAl-LDH-F-36 are the priority nucleation center for Au nanoparticles. It can be considered as the above mentioned "dangling orbital" with high energy at the edges of the "flower petals".[18] After loading, surface hydrogen vacancies are almost completely covered by AuNPs or eliminated by filling in hydrogen species from the decomposition of overweight $NaBH_4$, which leads to the disappearance of the characteristic peak. Furthermore, the BE value of the Ni $2p_{3/2}$ electron in fresh Au/NiAl-LDH-F-36 is slightly higher than that in the fresh support, indicating that there is a slight electron transfer from Ni species to AuNPs because of the higher electronegativity of Au.

In Fig. 5A, the peaks of $Ni^{2+}$-OH, $Ni^{3+}$-OH in Ni $2p_{3/2}$ binding energy (BE) are distinguished in these samples, as well as $Au^0$, $Au^+$ and $Au^{3+}$ in Au $4f_{7/2}$.[12, 13, 23-25] Significantly, the BE value of metallic Au is 82.9 eV, and remarkably lower than 84.0 eV, which is mainly because of the electron donation from supports.[2, 26, 27] Besides, the recycle process of $Ni^{2+}\leftrightarrow Ni^{3+}$ in the whole reaction cycle is in accordance with the recent reports.[12, 23] However, we find that the valent cycle of Au species is different from that reported in other Au-Ni system which is often considered as the process of $Au^0\leftrightarrow Au^+$.[12, 23] In as-synthesized fresh catalyst, Au species present two different types assigned to $Au^0$ and cationic $Au^+$. However, experiencing pretreatment, a new peak caused by $Au^{3+}$ species is observed.

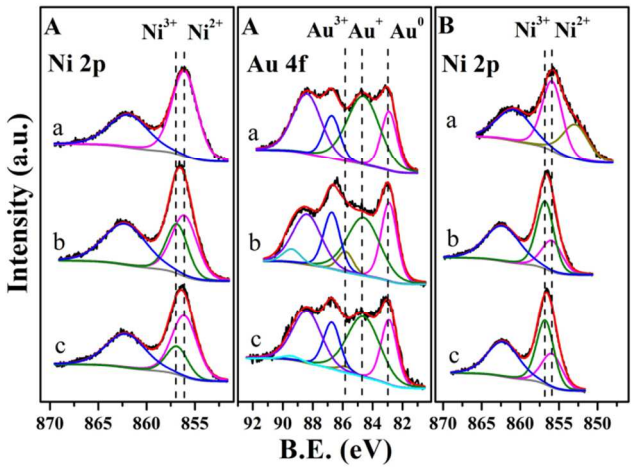


**Fig. 5** XPS spectra in Ni 2p or Au 4f regions on the flower-like catalyst (A) and corresponding support (B) surface: the fresh sample (a), the pretreated sample (b), the pretreated sample experienced the oxidation of benzyl alcohol at reaction conditions (c).

Meanwhile, the amount of $Au^+$ species decrease from 70.37% to 54.94%, while the amount of $Au^0$ species remained about the same. Therefore, we speculate that during calcination, $Au^+$-$Ni^{2+}$ hybrid species are oxidized to $Au^{3+}$-$Ni^{3+}$ ones in which the $Au^{3+}$ species can be stabilized on the LDH surface by $Ni^{3+}$ and oxygen-deficient sites.[25] In addition, after reaction, the peak of $Au^{3+}$ species almost disappears, which means $Au^{3+}$-$Ni^{3+}$ hybrid species could be reduced by alcohols to $Au^+$-$Ni^{2+}$ ones during the reaction.

Through the XPS data, more details are proved in the mechanism of BA oxidation. After pretreatment, the work function of catalyst reveals upward trend due to the formation of $Ni^{3+}$ and $Au^{3+}$, resulting in the increase of electron transfer from benzyl alcohol to the catalyst.[28, 29] In benzyl alcohol molecules, alcoholic hydroxyl groups as the origins of transferred electron undergo coordination with catalyst to form an unsteady alkoxide intermediate for further elimination of β-H. Hence, the transformation of $Ni^{2+}\rightarrow Ni^{3+}$ and $Au^+\rightarrow Au^{3+}$ can promote the determined step of alcoholic oxidations. Moreover, the isolated $Au^{3+}$ cations make a great contribution to the reaction between active $O^*$ adspecies with hydride. $Au_2O_3$ is composed of a network of identical $AuO_4$ units in which the Au ion breaks two Au-O bonds and binds to one oxygen atom of the $O_2$ adsorbed in the oxygen vacancy at metal-support perimeter interface.[30-33] The hydride spilled over from support could react with this active oxygen adspecies.[34] On these bases, we propose that the $Au^{3+}$-$Ni^{3+}$ hybrid site is the reaction center possessing dramatically higher activity, which has been proved by the rising yield form 13% to 53% after pretreatment.

Furthermore, the metabolic oxidation state of Ni species in the pristine NiAl-LDH-F-36 support was also inspected in the whole reaction recycle as shown in Fig. 5B. It is worth noticing that $Ni^{3+}$ species cannot be reduced to $Ni^{2+}$ in the oxidation reactions, indicating that, without Au species, active $O^*$ adspecies stored at O vacancies on the surface of support could not join into the reaction.

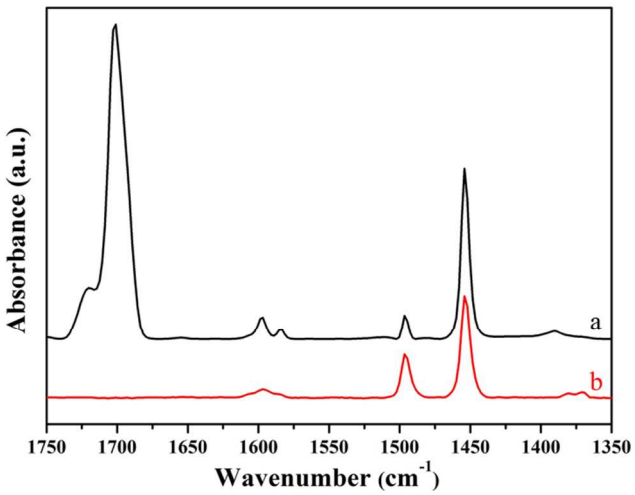


**Fig. 6** DRIFT spectra of benzyl alcohol dosed Au/NiAl-LDH-F-36 catalyst (a) and NiAl-LDH-F-36 support (b) at 100 °C.

Although a number of researches have proposed possible mechanisms in the system of Au/LDH,[3, 29, 35] to the best of our knowledge, the concrete evidences are still not given. DRIFT spectroscopic studies were performed on Au/NiAl-LDH-F-36 catalyst and NiAl-LDH-F-36 support dosed with small quantities of BA. The spectra are shown in Fig. 6 and the detailed band information are shown in Table S2. For both samples, bands associating with aromatic C=C and C-H modes (1454 $cm^{-1}$, 1496 $cm^{-1}$, 1584 $cm^{-1}$, 1596 $cm^{-1}$, 1598 $cm^{-1}$ and 1606 $cm^{-1}$) are observed. In the low-frequency region, all bands centered from 1360 $cm^{-1}$ to 1400 $cm^{-1}$ indicate the perturbation of the adsorbed hydroxyl groups of BA.[36, 37] However, obvious differences in the peak position and quantity are demonstrated in both samples, indicating the different interactions between BA and the adsorbing sites. In NiAl-LDH-F-36 support, it is known that BA adsorbs on the Brønsted base sites[29, 35] in two modes, on $Ni^{2+}$-OH (1370 $cm^{-1}$) and $Ni^{3+}$-OH (1380 $cm^{-1}$) sites. However, in Au/NiAl-LDH-F-36, only a tailing peak with significant blue shift appears in this range with a maximum at 1390 $cm^{-1}$, suggesting that Au cations further promotes the electron transfer from alcoholic hydroxyl groups to catalysts. In other words, all the Brønsted base sites, $Ni^{III}$ CUS and Au cations in the system of Au/NiAl-LDH-F-36 make the contributions to the β-H eliminate for enhancing the activity. In addition, it is worth noticing that in the high-frequency region, no signals are present between 1650 $cm^{-1}$ and 1750 $cm^{-1}$ in NiAl-LDH-F-36 support. However, the signals of carbonyl bands in Au/NiAl-LDH-F-36 centered at 1702 and 1720 $cm^{-1}$ clearly appear and belong to BD. The appearance of these bands implies that the production of BD strongly adsorbs on the catalyst, which reconfirms that without the assistance of AuNPs, active $O^*$ adspecies could not join into the reaction.

### Mechanistic investigation

Based on our experimental results, we proposed a possible mechanism with $Au^{3+}$-$Ni^{3+}$-OH as a hybrid active site (Scheme 2). In the pretreatment process, $Ni^{2+}$ and $Au^{+}$ are oxidized to $Ni^{3+}$ and $Au^{3+}$, respectively. Meanwhile, oxygen molecules are adsorbed and activated to active $O^*$ species which are further stored in the O vacancies at metal-support perimeter interface. At the beginning of reaction, BA molecules attack basic Ni-OH sites to give an alkoxide intermediate. Subsequently, the intermediate undergoes coordination to afford unsteady metal-alcoholate-species, which is considered as the rate-determining step and promoted by both $Ni^{III}$ CUS and Au cations, leading to the elimination of β-H. The final step is the rapid oxidation of

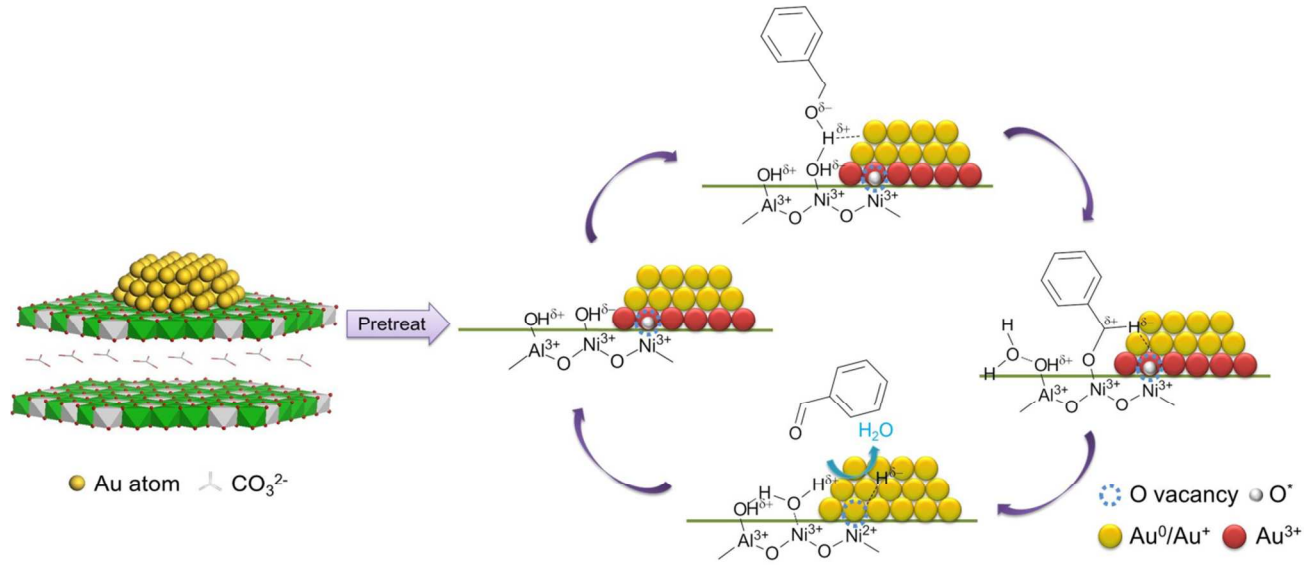


**Scheme 2** The possible reaction pathway of the oxidation for benzyl alcohol over Au/NiAl-LDH catalyst.

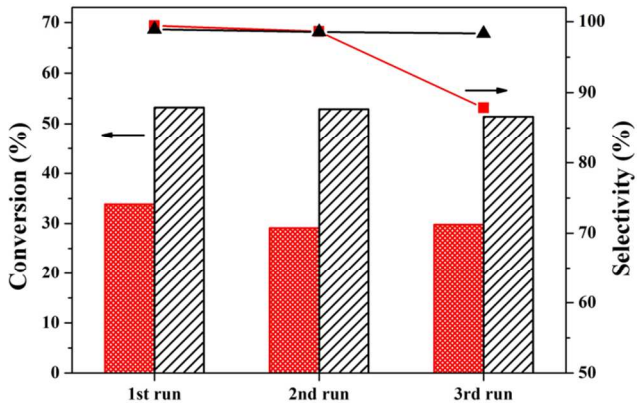


**Fig. 7** Reusability of Au/NiAl-LDH-P-36 (red) and Au/NiAl-LDH-F-36 (black).

the hydride by active O*. Along with the consumption of active O* adatoms, the $Au^{3+}$-$Ni^{3+}$ hybrid site is reduced to the $Au^{+}$-$Ni^{2+}$. With the desorption of BD and water molecules, the catalytic cycle is thereby completed. According to this reaction mechanism, both hydroxyl arrays and the synergy between Ni and Au play as the key factors for the enhancement of activity.[18]

### Recyclability of various catalysts

The reusability of the catalysts was investigated for three successive reactions as shown in Fig. 7. There is a considerable decrease of activity (nearly 12%) over the Au catalyst with common nanoparticle NiAl-LDH-P-36 support in the 3rd run comparing with the 1st. However, the Au/NiAl-LDH-F-36 catalyst with flower-like support only shows around 4% deactivation after the 3rd run. The HRTEM images of the used Au catalysts demonstrate that the aggregation from 2.45 nm to 4.58 nm is the key reason for the activity loss in Au/NiAl-LDH-P-36 (Fig. S5). In contrast, the aggregation of AuNPs in Au/NiAl-LDH-F-36 is rarely conspicuous. However, the aggregation of AuNPs cannot explain the obvious decrease of selectivity and tiny increase of activity in the 3rd run, thereby ICP was taken for the catalysts after recycle. The results suggest that the leaching of AuNPs from support to solution becomes the reason for the side reactions (Table 1).[38] Thereupon, the remarkable recyclability of the flower-like catalyst with almost full reusability has been highlighted by contrast, resulting from the perpendicularly interlaced morphology of "flower petals" which can facilitate the immobilization of nano-metallic particles for avoiding the possible aggregation and leaching.[4] In summary, the hierarchical Au/NiAl-LDH catalyst possesses not only higher activity but also preferable stability during the oxidation of benzyl alcohol.

### Various catalytic aerobic oxidation of alcohols over AuNPs supported on flower-like NiAl-LDH

To obtain more information about hierarchical catalysts, the

**Table** 2 Aerobic oxidation of various alcohols using Au/NiAl-LDH.

| Entry | Substrate | Main Product[c] | Catalyst | Temperature (°C) | TOF ($h^{-1}$) | Ref. |
|---|---|---|---|---|---|---|
| 1[a] | Crotonyl alcohol | Crotonic acid | Au/NiAl-LDH-P-36 | 100 | 45 | this work |
| 2[a] | | | Au/NiAl-LDH-F-36 | 100 | 45 | this work |
| 3[a] | 1-octanol | 1-octoic acid | Au/NiAl-LDH-P-36 | 100 | 123 | this work |
| 4[a] | | | Au/NiAl-LDH-F-36 | 100 | 126 | this work |
| 5[a] | Cinnamic alcohol | Cinnamyl aldehyde | Au/NiAl-LDH-P-36 | 100 | 148 | this work |
| 6[a] | | | Au/NiAl-LDH-F-36 | 100 | 239 | this work |
| 7[a] | 4-Methylbenzyl alcohol | 4-Methyl benzaldehyde | Au/NiAl-LDH-P-36 | 100 | 259 | this work |
| 8[a] | | | Au/NiAl-LDH-F-36 | 100 | 347 | this work |
| 9[a] | Cyclohexanol | Cyclohexanone | Au/NiAl-LDH-P-36 | 100 | 101 | this work |
| 10[a] | | | Au/NiAl-LDH-F-36 | 100 | 225 | this work |
| 11[a] | Benzhydrol | Benzophenone | Au/NiAl-LDH-P-36 | 100 | 309 | this work |
| 12[a] | | | Au/NiAl-LDH-F-36 | 100 | 445 | this work |
| 13[b] | Benzyl alcohol | Benzaldehyde | Au/NiAl-LDH-P-36 | 140 | 8023 | this work |
| 14[b] | | | Au/NiAl-LDH-F-36 | 140 | 10026 | this work |
| 15 | | | Au/MgAl-MMO | 140 | ~4500 | 3 |
| 16 | | | Au/SBA-16 | 140 | 1937 | 39 |
| 17 | | | $AuPd/TiO_2$ | 140 | 6420 | 40 |
| 18 | | | AuPd/C | 140 | 7830 | 40 |
| 19 | | | $Au/TiO_2$ | 160 | 12400 | 41 |

[a] The reaction conditions are the same as those in Table 1.

[b] Reaction conditions: benzyl alcohol (1 mL), catalysts (10 mg), $O_2$ (0.1 MPa), 140 °C, 0.5 h, 1000 rpm, 50 mL glass stirred reactors.

[c] Determined by GC-MS.

Journal Name RSCPublishing

ARTICLE

oxidation of various typical alcohols was evaluated in toluene as shown in Table 2. We note that Au/NiAl-LDH-F-36 can oxidize a wide range of alcohols to the corresponding carbonyl compounds with higher activity than Au/NiAl-LDH-P-36 except for crotonyl alcohol and 1-octanol which are both linear alcohols. The similar TOFs in each group suggest that the effective collision between linear alcohols and active sites cannot be enhanced in the straight macro-pores. It is worth noticing that the effective collision can also be enhanced in the benzhydrol oxidation of which the molecule size is beyond 1 nm, although the increase amount of TOF is relatively lower than others. It is mainly attributed to the steric constraint for the bulky molecule structure with bigger size.

Distinctively, considering that toluene is a byproduct in BA oxidation, the solvent-free oxidation of BA was thus tested. The TOF of Au/NiAl-LDH-F-36 is 25% higher than Au/NiAl-LDH-P-36, which results from the special hierarchitecture as mentioned above. Moreover, the TOF (10025 $h^{-1}$) of Au/NiAl-LDH-F-36 is much higher than previously reports such as ~4500 $h^{-1}$ of Au/MgAl-MMO[3], 1937 $h^{-1}$ of Au/SBA-16[39], and even higher than 6420 $h^{-1}$ of AuPd/$TiO_2$ and 7830 $h^{-1}$ of AuPd/C which are both regarded as two types of the most efficient catalysts for oxidation at present[40]. Significantly, the TOF of Au/NiAl-LDH-F-36 at 140 $^oC$ is comparable with 12400 $h^{-1}$ of the Au/$TiO_2$ catalyst at 160 $^oC$[41]. All superiorities are brought from the combination of hierarchitecture, Au-Ni synergy and hydroxyl arrays.

## Conclusions

In this work, a one-step hydrothermal method was utilized for the synthesis of flower-like NiAl-LDH with outer trumpet-like hierarchical pore structure. XPS results indicated that abundant hydrogen vacancies at the edge of "flower petals" provided the nucleation centers for AuNPs in the process of sol-immobilization, resulting in the uniform dispersion of AuNPs. As comparison, common particle Au/NiAl-LDH catalyst was also synthesized. The catalytic performance of flower-like Au/NiAl-LDH catalyst and the contrastive one were tested in the selective oxidation of benzyl alcohol. By contrast, the activity of flower-like catalyst was dramatically enhanced by 60% due to confinement effect of the hierarchical pores which increase the effective collisions between substrates and active sites. Besides, the influence of pretreatment was also investigated. After pretreatment in air, $Au^+$-$Ni^{2+}$ hybrid sites at interface perimeter were partially oxidized to $Au^{3+}$-$Ni^{3+}$ as more active reaction centers, which led to further increase in activity. The cooperation of the Brønsted base sites, $Ni^{III}$ CUS, and isolated gold cations in the system for the β-H eliminate of benzyl alcohol was proved by DRIFT analysis and the rational reaction route was therefore clarified. Moreover, the oxidations of other alcohols in various types were further measured and the as-fabricated flower-like catalyst also performed more effective than the common nanoparticle one in the most oxidations except for in linear alcohols, which is attributed to the shape selectivity of straight macro-pores by affecting the effective collision between active sites and substrates. We believe that the synthesized hierarchical multifunctional catalyst in this work could offer a novel strategy for designing high performance catalysts for green, hypotoxicity and efficient oxidations.

## Experimental

### Preparation of supported Au/LDH catalysts

#### Synthesis of LDH support

The hierarchical NiAl-LDHs with different $[Ni^{2+}]/[Al^{3+}]$ molar ratio were synthesized by a urea decomposition method with the assistance of $NH_4F$ as morphology control agent similar as that ascribed by Wei et al[16]. In brief, the $Ni(NO_3)_2{\cdot}6H_2O$ (0.006 M), $Al(NO_3)_3{\cdot}9H_2O$ (0.002 M), urea (0.04 M) and $NH_4F$ (0.016 M) were dissolved in deionized water (100 mL) to give a transparent solution. The resulting solution was aged in sealed-Teflon autoclave at 110 $^oC$ for 36 h. The precipitations were washed until pH reached 7 with water and dried at 60 $^oC$ overnight. The as-synthesized NiAl-LDH was denoted as NiAl-LDH-F-36. Considering the effects brought from synthesized duration for LDH structures, hydrothermal time was shortened to 24 h and 12 h which were called NiAl-LDH-F-24 and NiAl-LDH-F-12, respectively. The other processes were taken like ones in preparing NiAl-LDH-F-36. The nanoparticle NiAl-LDH was obtained similarly as NiAl-LDH-F-36 without $NH_4F$ with the name NiAl-LDH-P-36. MgAl-LDH-P-36 was synthesized analogously as NiAl-LDH-P-36 with the only replacement of $Ni(NO_3)_2{\cdot}6H_2O$ to $Mg(NO_3)_2{\cdot}6H_2O$ in the same proportion.

#### Synthesis of Au/LDH catalyst

All the supported Au/LDH catalysts were prepared by the sol-immobilization method. An aqueous solution of hydrogen tetrachloroaurate (III) trihydrate ($HAuCl_4{\cdot}3H_2O$, AR) with the desired concentration was stirred with magnetic force which was named as solution A. The required amount of a PVA solution (1 wt.%) was added into the solution A (PVA/Au=2 wt./wt.), then a freshly prepared solution of $NaBH_4$ (0.1 M) was dumped quickly ($NaBH_4$/Au=5 mol/mol) to form a dark-brown

sol. After the sol generation with 30 min, the reducible AuNPs was immobilized by adding support of which requirement was calculated so as to have a total final metal loading of 1% wt. After 1 h the slurry was filtered, the catalyst washed thoroughly with acetone and deionized water followed by drying at 80 $^{o}$C overnight.

### Catalyst characterization

The morphology and structure of the samples were examined using a Zeiss Supra 55 scanning electron microscope (SEM). X-ray diffraction (XRD) patterns were performed by a Shimadzu XRD-6000 diffractometer using Cu Kα source (λ= 0.154 nm) in the 2θ range from 3° to 70° and a scan step of 10° min$^{-1}$.The lattice fringes of the catalysts were characterized using a JEOL JEM-2100 high-resolution transmission electron microscope (HRTEM). Information on the pore structure of as-synthesized samples was obtained by mercury intrusion porosimetry (MIP) using a pore-size analyzer (PoreMasterGT 60, Quantachrome Inc.), which measures the amount of mercury penetration as a function of the applied pressure. The Brunauer-Emmett-Teller (BET) method is based on the adsorption isotherm. The Barrett-Joyner-Halenda (BJH) method was used to calculate the pore volume and the pore size distribution. Chemical analyses were obtained with inductively coupled plasma emission spectroscopy (ICP-AES; a Shimadzu ICPS-75000).

X-ray photoelectron spectroscopy (XPS) of the samples was collected using a Thermo VG ESCALAB 250 spectrometer equipped with Al Kα anode. The calibration peak is the C 1s peak at 284.6 eV. DRIFT spectroscopy studies were performed using a Bruker Tensor 27 spectrometer fitted with a high sensitivity MCT detector and a diffusIR heated chamber equipped with KBr windows. Samples were pretreated with $O_2$ at 200 $^{o}$C for 1 h and then cooled down with $N_2$. After an initial scan at 100 $^{o}$C in $N_2$ flow under atmosphere as the background, benzyl alcohol was added by an in-line saturator heated to 150 $^{o}$C for 1 h. Experiencing the purge in $N_2$ for 1 h, spectra were run in the range of 4000-600 cm$^{-1}$ with 64 accumulation scans at 100 $^{o}$C.

### Catalytic reactions

The liquid-phase aerobic oxidations of various alcohols with solvent were carried out using a 50 mL three-necked round-bottle flask with a reflux condenser. Most of the as-fabricated catalysts were pretreated at 200 $^{o}$C for 30 min in air. Each oxidized process charged with of alcohol (1.0 mmol), toluene (10 mL) and catalysts (0.05 g). Molecular oxygen was bubbled through the reaction mixture (20 mL min$^{-1}$). The resulting mixture was heated at 100 $^{o}$C for 0.5 h timing after reaching 100 $^{o}$C and then cooled with ice bath. The suspension was separated by centrifugation and washed with acetone for several times. After drying at 80 $^{o}$C for 30 min, the recycled catalyst can be reused in the next run under the same conditions. The reaction products were analyzed by a Agilent J&W GC-FID (DB-Wax, 30 m × 0.320 mm, $d_f$ = 0.25 μm) using an external standard technique. Mesitylene was used as external standard for GC analysis. In all cases, the carbon balances were 100±5%.

## Acknowledgements

This work was supported by National Natural Science Foundation, the 973 Project (2011CBA00506), Beijing Natural Science Foundation (2132032), the Fundamental Research Funds for the Central Universities (YS1406) and the Beijing Engineering Center for Hierarchical Catalysts.

## Notes and references

* State Key Laboratory of Chemical Resource Engineering, Beijing University of Chemical Technology, Box 98, 15 Bei San Huan East Road, Beijing 100029, China.
E-mail: fengjt@mail.buct.edu.cn, lidq@mail.buct.edu.cn

Electronic Supplementary Information (ESI) available: [details of any supplementary information available should be included here]. See DOI: 10.1039/b000000x/

1 P. Liu, Y. Guan, R. A. van Santen, C. Li and E. J. Hensen, *Chem. Commun.*, 2011, **47**, 11540.
2 P. Liu, V. Degirmenci and E. J. M. Hensen, *J. Catal.*, 2014, **313**, 80.
3 J. Feng, C. Ma, P. J. Miedziak, J. K. Edwards, G. L. Brett, D. Li, Y. Du, D. J. Morgan and G. J. Hutchings, *Dalton Trans.*, 2013, **42**, 14498.
4 F. Mi, X. Chen, Y. Ma, S. Yin, F. Yuan and H. Zhang, *Chem. Commun.*, 2011, **47**, 12804.
5 A. Abad, P. Concepción, A. Corma and H. García, *Angew. Chem. Int. Ed.*, 2005, **44**, 4066.
6 S. A. Kondrat, G. Shaw, S. J. Freakley, Q. He, J. Hampton, J. K. Edwards, P. J. Miedziak, T. E. Davies, A. F. Carley and S. H. Taylor, *Chem. Sci.*, 2012, **3**, 2965.
7 W. Hou, N. A. Dehm and R. W. J. Scott, *J. Catal.*, 2008, **253**, 22.
8 R. Dun, X. Wang, M. Tan, Z. Huang, X. Huang, W. Ding and X. Lu, *ACS Catal.*, 2013, **3**, 3063.
9 S. E. Davis, M. S. Ide and R. J. Davis, *Green Chem.*, 2013, **15**, 17.
10 G.-J. ten Brink, I. W. Arends and R. A. Sheldon, *Science*, 2000, **287**, 1636.
11 L.-C. Wang, Y.-M. Liu, M. Chen, Y. Cao, H.-Y. He and K.-N. Fan, *J. Phys. Chem. C*, 2008, **112**, 6981.
12 G. Zhao, H. Hu, M. Deng and Y. Lu, *Chem. Commun.*, 2011, **47**, 9642.
13 A. Villa, C. E. Chan‐Thaw, G. M. Veith, K. L. More, D. Ferri and L. Prati, *ChemCatChem*, 2011, **3**, 1612.
14 G. Zhao, H. Hu, W. Chen, Z. Jiang, S. Zhang, J. Huang and Y. Lu, *Catal. Sci. Technol.*, 2013, **3**, 404.
15 P. Xu, R. Yu, H. Ren, L. Zong, J. Chen and X. Xing, *Chem. Sci.*, 2014, **5**, 4221.
16 C. Li, Y. Dou, J. Liu, Y. Chen, S. He, M. Wei, D. G. Evans and X. Duan, *Chem. Commun.*, 2013, **49**, 9992.
17 V. Prevot, N. Caperaa, C. Taviot-Guého and C. Forano, *Cryst. Growth Des.*, 2009, **9**, 3646.
18 F. Zhang, X. Zhao, C. Feng, B. Li, T. Chen, W. Lu, X. Lei and S. Xu, *ACS Catal.*, 2011, **1**, 232.

19 C. M. Nguyen, M.-F. Reyniers and G. B. Marin, *J. Catal.*, 2015, **322**, 91.
20 C. M. A. Parlett, K. Wilson and A. F. Lee, *Chem. Soc. Rev.*, 2013, **42**, 3876.
21 Q. Xie, Y. Zhao, X. Chen, H. Liu, D. G. Evans and W. Yang, *Biomaterials*, 2011, **32**, 6588.
22 W. J. Ong, L. L. Tan, S. P. Chai, S. T. Yong and A. R. Mohamed, *Nanoscale*, 2014, **6**, 1946.
23 G. Zhao, J. Huang, Z. Jiang, S. Zhang, L. Chen and Y. Lu, *Appl. Catal. B Environ.*, 2013, **140-141**, 249.
24 P. Concepción, S. Carrettin and A. Corma, *Appl. Catal. A Gen.*, 2006, **307**, 42.
25 L.-F. Gutiérrez, S. Hamoudi and K. Belkacemi, *Appl. Catal. A Gen.*, 2012, **425–426**, 213.
26 H. Tsunoyama, N. Ichikuni, H. Sakurai and T. Tsukuda, *J. Am. Chem. Soc.*, 2009, **131**, 7086.
27 F. Wang, W. Ueda and J. Xu, *Angew. Chem. Int. Ed.*, 2012, **51**, 3883.
28 T. Dutta, P. Gupta, A. Gupta and J. Narayan, *J. Phys. D: Appl. Phys.*, 2010, **43**, 105301.
29 W. Fang, J. Chen, Q. Zhang, W. Deng and Y. Wang, *Chem. Eur. J.*, 2011, **17**, 1247.
30 M. F. Camellone and S. Fabris, *J. Am. Chem. Soc.*, 2009, **131**, 10473.
31 H. Shi, R. Asahi and C. Stampfl, *Phys. Rev. B*, 2007, **75**, 205125.
32 N. Weiher, E. A. Willneff, C. Figulla-Kroschel, M. Jansen and S. L. M. Schroeder, *Solid State Commun.*, 2003, **125**, 317.
33 M. Haruta, *Cattech*, 2002, **6**, 102.
34 C.-T. Chang, B.-J. Liaw, Y.-P. Chen and Y.-Z. Chen, *J. Mol. Catal. A: Chem.*, 2009, **300**, 80.
35 T. Chen, F. Zhang and Y. Zhu, *Catal. Lett.*, 2013, **143**, 206.
36 E. Nowicka, J. P. Hofmann, S. F. Parker, M. Sankar, G. M. Lari, S. A. Kondrat, D. W. Knight, D. Bethell, B. M. Weckhuysen and G. J. Hutchings, *Phys. Chem. Chem. Phys.*, 2013, **15**, 12147.
37 C. Keresszegi, D. Ferri, T. Mallat and A. Baiker, *J. Phys. Chem. B*, 2004, **109**, 958.
38 D. V. Bavykin, A. A. Lapkin, S. T. Kolaczkowski and P. K. Plucinski, *Appl. Catal. A Gen.*, 2005, **288**, 175.
39 Y. Chen, H. Lim, Q. Tang, Y. Gao, T. Sun, Q. Yan and Y. Yang, *Appl. Catal. A Gen.*, 2010, **380**, 55.
40 Q. He, P. J. Miedziak, L. Kesavan, N. Dimitratos, M. Sankar, J. A. Lopez-Sanchez, M. M. Forde, J. K. Edwards, D. W. Knight, S. H. Taylor, C. J. Kiely and G. J. Hutchings, *Faraday Discuss.*, 2013, **162**, 365.
41 D. I. Enache, J. K. Edwards, P. Landon, B. Solsona-Espriu, A. F. Carley, A. A. Herzing, M. Watanabe, C. J. Kiely, D. W. Knight and G. J. Hutchings, *Science*, 2006, **311**, 362.



 